Tailored and Guided Dewetting of Block Copolymer/Homopolymer Blends

Tailored and Guided Dewetting of Block Copolymer/Homopolymer Blends

F. Ferrarese Lupi,[1] I. Murataj,[1-2] F. Celegato,[1] A. Angelini,[1-2] F. Frascella,[2] R. Chiarcos,[3] D. Antonioli,[3] V. Gianotti,[3] P. Tiberto,[1] C. F. Pirri,[2] L. Boarino,[1] M. Laus [3]*

[1] *Nanoscience and Materials Division, Istituto Nazionale Ricerca Metrologica, Strada delle Cacce 91, 10135 Torino, Italy*

[2] *Dipartimento di Scienza Applicata e Tecnologia, Politecnico di Torino, Corso Duca degli Abruzzi, 24, 10129 Torino, Italy*

[3]*Dipartimento di Scienze e Innovazione Tecnologica (DISIT), Università del Piemonte Orientale ''A. Avogadro'', Viale T. Michel 11, 15121 Alessandria, Italy*

Corresponding author e-mail: f.ferrareselupi@inrim.it

KEYWORDS: Block Copolymers, Dewetting, Block Copolymer/Homopolymer Blend, Rapid Thermal Processing, Self-assembly, Hierarchical Patterns.

For Table of Contents use only

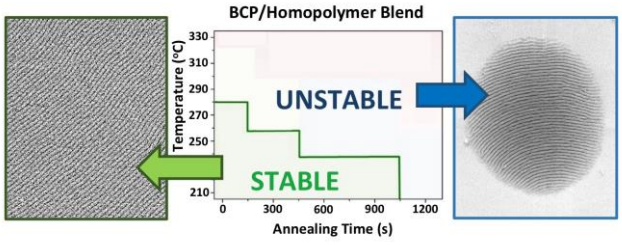

ABSTRACT

The dewetting and ordering characteristics of a lamellae forming poly(styrene-block-methyl methacrylate) (PS-b-PMMA) block copolymer (BCP) either alone or blended with low molecular weight polystyrene (PS) and polymethylmethacrylate (PMMA) homopolymers were investigated. Although a significant reduction of the morphological stability is observed for the blend BCP compared to the neat BCP, an increase of one order of magnitude occurs in the correlation length of the lamellar nano-domains. Moreover, the morphological instability of blend BCP results in dewetting of relatively thick films with the formation of micrometric size areas consisting of highly ordered and defect free perpendicular lamellae monodomains. These results can be exploited for large-scale manufacturing of BCP-based plasmonic and optical structures featuring substantial thickness-modulation.

INTRODUCTION

Block copolymer self-assembly represents a most interesting tool in the preparation of nanostructures for optical applications. The self-assembly of BCP revealed highly efficient in the creation of a wide variety of photonic materials prepared from lamellar, cylinder as well as gyroid morphologies.[1-2-3-4] However, the lack of precise control over the intrinsically stochastic nature of the self-assembly process represents the bottleneck to large scale manufacturing of BCP-based optical devices.

A technology based on the induction of dewetting in thin BCP films over patterned surfaces was recently proposed as an effective method to obtain highly ordered hierarchical structures, even with curved shapes.[5-6-7] This approach took advantage from the extensive optimization of the key factors exploiting the block copolymer self-assembly for nanolithography. For this application, an unpreceded level of control was achieved by developing surface tailoring approaches to control the block copolymer nanofeature orientation and by using patterned surfaces to precisely register the nanostructures, propagate the correlation over very long distances and suppress or reduce defect formation.[8-9] Unfortunately, dewetting based strategies rely on the intrinsic instability of very thin BCP films (*i.e.* thickness $h < 10$

nm), thus limiting the preparation of high aspect-ratio self-assembled structures and thickness-modulated nanometric patterns.[10-11] In addition, defects as disclinations and dislocations are observed inside the dewetted structures.

On the other hand, strong alignment of nanometric structures was demonstrated also in thick BCP films in the presence of a local thickness gradient, naturally induced in near-edge regions[12] or in films deposited under controlled casting conditions.[13] In the latter case, the preferential alignment of the lamellar nanostructures along the thickness gradient, ascribed to the "*geometric anchoring*" phenomenon, is limited to BCP films with contact angles θ > 3°-5° and h > 500 nm.[14] These geometric constraints are imposed by the reduced defect annihilation rate observed for values of h lower than 500 nm.

In this perspective, the defect density annihilation rate is remarkably speed up in both cylindrical[15-16] and lamellar[17] binary or ternary blends of BCP with homopolymers[18-19] as well as random[20] or even block copolymers.[21] In particular, the presence of homopolymers with molar mass (M_n) lower than M_n of the corresponding block in the BCP gives rise to a significant reduction of the energy barrier for the polymer chain diffusion and the morphological reorganization, leading to an appreciable reduction of defects by mutual annihilation.[20,22]

According to the above considerations, the present study focuses on topography and nanoscale ordering in the stability and dewetting regions of ternary blends consisting of a lamellae forming poly(styrene-block-methylmethacrylate) (PS-b-PMMA) BCP and low molar mass polystyrene (PS) and polymethylmethacrylate (PMMA) homopolymers. It can be anticipated that the presence of low molar mass homopolymers relaxes the *geometric anchoring* constraints and induces the dewetting of thicker films thus allowing the fabrication of defect free patterned structures featuring a substantial thickness-modulation. This finding represents a novel and powerful tool for large-scale manufacturing of BCP-based plasmonic and optical structures.

EXPERIMENTAL SECTION

Materials. Tert-Butyl α bromoisobutyrate, tris (2- (dimethylamino) ethyl) amine (Me_6TREN), tris (2-pyridylmethyl) amine (TPMA), copper (II) bromide ($CuBr_2$), tin (II) 2-ethylhexanoate (Sn $(EH)_2$) were purchased from Sigma Aldrich and used as received. Styrene and methyl methacrylate monomers were purchased from Sigma Aldrich and purified by an inhibitor remover (Sigma Aldrich) before use. All solvents were purchased from Sigma Aldrich. A PS-b-PMMA (BCP) with styrene fraction of 0.50, polydispersity index Đ = 1.09 and numeral average molecular weight (M_n) of 66 kg/mol was purchased from Polymer Source Inc. and used without further purification.

Polymers synthesis. An α-hydroxy ω-Br poly (styrene-random-methyl methacrylate) copolymer (RCP), named P(S-r-MMA), characterized by a numerical average molecular weight M_n = 14.60 kg/mol, a styrene fraction (f) of 0.59 and a polydispersity index (Đ) = 1.30, was synthesized as previously described.

The low molecular weight unreactive polystyrene sample, named $PS_{3.1}$, was synthesized by Activator ReGenerated by Electron Transfer-Atom Transfer Radical Polymerization (ARGET-ATRP), initiated by tert-Butyl α bromoisobutyrate and catalysed by $CuBr_2$ complexed by Me_6TREN ligand in presence of Sn $(EH)_2$ as reducing agent. The molar ratios between monomer, initiator, $CuBr_2$, Me_6TREN and Sn $(ET)_2$ were 100/1/0.02/0.22/0.2. The polymerization reaction was conducted for 2 hours at 90° C. The obtained polystyrene was characterized by a M_n = 3.1 kg/mol and Đ = 1.09.

The low molecular weight unreactive polymethyl methacrylate sample, named $PMMA_{3.9}$, was also synthesized by ARGET-ATRP employing the same initiator, catalyst and reducing agent of the polystyrene synthesis. The ligand was switched from Me_6TREN to TPMA. The molar ratios between monomer, initiator, $CuBr_2$, Me_6TREN and Sn $(ET)_2$ were 30/1/0.04/0.24/0.2. The polymerization reaction was conducted for 45 minutes at 70° C. The obtained polymethyl methacrylate was characterized by a M_n = 3.9 kg/mol and Đ = 1.18.

The synthesis of $PMMA_{3.9}$ sample is now described in detail as a typical example. A solution of $CuBr_2$ (22.4 mg, 100 µmol) and TPMA (30 mg, 100 µmol) in 4 ml of anisole was mixed with methyl

methacrylate (8 ml, 75 mmol) and initiator (470 µl, 2.5 mmol) in to a Schlenk flask. The solution was degassed by two freeze-thaw cycles and then a solution of Sn $(EH)_2$ (200 mg, 500 µmol) and TPMA (145 mg, 500 µmol) in 1 ml of anisole was added. Next another freeze-thaw cycle was made. The reaction was conducted at 70° C for 45 minutes. The reaction temperature was then lowered to room temperature and the product was isolated by precipitation in cold methanol.

Random copolymer and homopolymers molecular weights were determined by Size Exclusion Chromatography (SEC) using tetrahydrofuran as eluent.

TGA-GC-MS Analysis. The TGA–GC–MS set-up was described in detail in ref. 23. Briefly, the polymeric films were located on the thermo-balance plate of a Mettler TGA851e TGA. GC–MS stage was performed by FINNIGAN TRACE GC-ULTRA and TRACE DSQ. The separation was obtained by a DB5-5ms capillary column (Phenomenex, 30 m, 0.25 mm i.d., 0.25 µm thickness). The injector was set in splitless mode at 250 °C (helium as carrier at 1.0 mL min^{-1}). MS transfer line and oven were set at 280 and 150 °C, respectively. The two transfer lines from TGA to the GC were at 200 °C and the interface was at 150 °C. The injection loop was 2.5 mL of volume and was filled after 10 s. EI^+ mode with ionization energy of 70.0 eV were used to obtain mass spectra with 250 °C of ion source temperature. Full-scan mode from 20 to 350 m/z, and selected ion monitoring (SIM) mode (S at 104 m/z and MMA at 100 m/z) were employed in the mass acquisition. The samples was heated at 20 °C min^{-1} from 25 to 600 °C with TGA–GC–MS analyses accomplished by repetitive (every 30 s) injections in the GC of 1.0 mL of the gas evolved from the TGA furnace.

Substrate neutralization. Substrate cleaning and activation were performed exposing the Si wafers with Silicon wafers covered by 1.5 nm thick native oxide layers were cleaned and activated by O_2 plasma treatment at 130 W for 6 minutes. A solution of P(S-r-MMA) (18 mg in 2 ml of toluene) was spin-coated onto the Si wafers at 3000 rpm for 60 s.[24] The grafting to process was induced by annealing in a rapid thermal processing (RTP) machine at high temperature (T_a = 290 °C) for an annealing time (t_a) of 300 s.

Afterwards, the non-grafted chains were removed by sonication for 6 min in a toluene bath, obtaining a RCP grafted layer with thickness of ~ 7 nm, determined by ellipsometry (alpha-SE ellipsometer, J.A. Wollam Co.).

BCP deposition. A BCP solution (9 mg/ml in toluene) was spin-coated (3000 rpm, 60 s) over the RCP-neutralized substrates to obtain the neat BCP series. A solution consisting of 4.5 mg of BCP, 1.12 mg of $PS_{3.1}$ and 1.12 mg of $PMMA_{3.9}$ in 1 ml of toluene was spin-coated (3000 rpm, 60 s) over the RCP-neutralized substrates to obtain the blend BCP series. The thickness of the layers was measured by ellipsometry (alpha-SE ellipsometer, J.A. Wollam Co.). All thermal treatments were made by RTP machine changing both the T_a and t_a. The lamellae opening process was performed by selective removal of the polymethyl methacrylate block from the polystyrene matrix obtained with an exposure of the samples to ultraviolet radiation (5 $mW \cdot cm^{-2}$, λ = 253.7 nm) for 180 s followed by isotropic O_2 plasma etching (40 W for 30 s).

TiO_2 nanowires were obtained by the selective infiltration of BCP films using the sequential infiltration synthesis (SIS) technique[25,26] inside an atomic layer deposition (ALD) machine (BENEQ TFS 200) at 135 °C. The timing sequence of the cyclical exposure of precursors consists on 600 s pulses of $TiCl_4$ and H_2O, followed by a 250 sccm N_2 purge step for 300 s. The polymer removal was subsequently performed by Ar plasma treatment (100 W for 600 s).

Graphoepitaxy patterns. Direct laser writer lithography (Heidelberg Laser Writer μPG101) is used in order to generate micrometric arrays of linear patterns with different size and periodicity over a 5 mm x 5 mm area. With this method, a commercial optical resist (AZ 5214E MicroChemicals GmbH) with 1 μm thickness, previously spin coated on the Si wafers, is exposed at a laser beam with 15 mW power and wavelength of 375 nm. After the exposure, the samples are immersed for 40 s in a 1:1 solution of AZ Developer (Merck Performance Materials GmbH) and deionized H_2O, and subsequently was rinsed in

H_2O for 60 s. The pattern transfer into the Si wafer is obtained by reactive etching process (RIE) with fluorine-based chemistry (C_4F_8 and SF_6). The final depth of the micrometric structures was set at 200 nm.

Morphology characterization. The homogeneity of the BCP films and the long-range ordering of the SA nanostructures were analyzed by a FEI Inspect-F field emission gun scanning electron microscope (FEG-SEM). In order to extract the correlation length values (ξ) the SEM micrographs were processed with a software routine following the conventional procedure described elsewhere.[27]

SEM micrographs were also used in order to classify the dewetted droplets in terms of area and circularity. To this goal SEM micrographs were binarized and the droplets were fitted with ellipses. The circularity was than calculated as the ratio between the minor and major axis of the resulting ellipses.

The topography of samples treated at different annealing conditions was investigated with a non-contact 3D surface profiler (S neox SENSOFAR) and a 150x confocal objective.

RESULTS AND DISCUSSION

To obtain the perpendicular lamellar morphology, an α-hydroxy poly(styrene-random-methyl methacrylate) random copolymer (RCP)[24] (M_n = 14.60 kg/mol, styrene fraction (f) of 58.7 (wt/wt) and polydispersity index (Đ) = 1.30) was grafted to the Si substrates. The grafting reaction, carried out in RTP[28-29] at 250°C for 900 s using the heating rate of 18 °C s^{-1}, leads to a RCP brush layer thickness of 7.6 nm.

Two sample sets were prepared for the topography and morphology analysis once subjected to the appropriate thermal treatments. The first set was obtained by spin coating, on the modified Si substrates, a PS-b-PMMA (M_n = 66 kg/mol, Đ = 1.09) block copolymer solution. The resulting set is marked as neat BCP. The second set was prepared by spin coating, on the modified Si substrates, a BCP/homopolymer blend solution prepared by mixing the same BCP with low molar mass polystyrene (M_n = 3.1 kg/mol, Đ = 1.09) and polymethyl methacrylate (M_n = 3.9 kg/mol, Đ = 1.18) homopolymers. This set was marked as blend BCP. To keep the lamellar structure while avoiding the formation of microemulsions or microphase

separated morphologies,[30] equal weights of BCP and homopolymers were employed and, in addition, the same weight of the two homopolymers was employed. For both sets, the spin-coating parameters were adjusted to obtain films with thickness $h \sim$ 40 nm

Both neat BCP and blend BCP sets were RTP treated with annealing time (t_a) and temperature (T_a) ranging from 30 to 1200 s and from 210 to 330 °C, respectively. To avoid spurious effects related to minor differences in the thermal conditions, one neat BCP and one blend BCP sample were thermally treated in each run.

Once processed, all the samples were analysed by optical profilometry and scanning electron microscopy (SEM) and classified according to the surface topography and nanoscale self-assembly characteristics. For completeness, all the SEM micrographs describing the nanometric lamellar structure of neat BCP and blend BCP are included in Figures S1 and S2, respectively.

Figure 1 reports the stability diagrams for neat BCP and blend BCP as a function of the annealing parameters (i.e. T_a and t_a). When the surface topography after the annealing treatment is flat and homogeneous (Figure 1a) the thin polymeric film is defined as stable. This condition is indicated by the green triangles in Figures 1c and 1d. In contrast, when the surface topography includes discontinuities and holes (see for example Figure 1b), the corresponding condition is defined as unstable.

The unstable morphologies are further differentiated by considering the early formation of topographic inhomogeneities (yellow squares in Figures 1c and 1d), the dewetting of the film (blue full circles) and the disappearance of lamellar nanostructures (red empty circles).

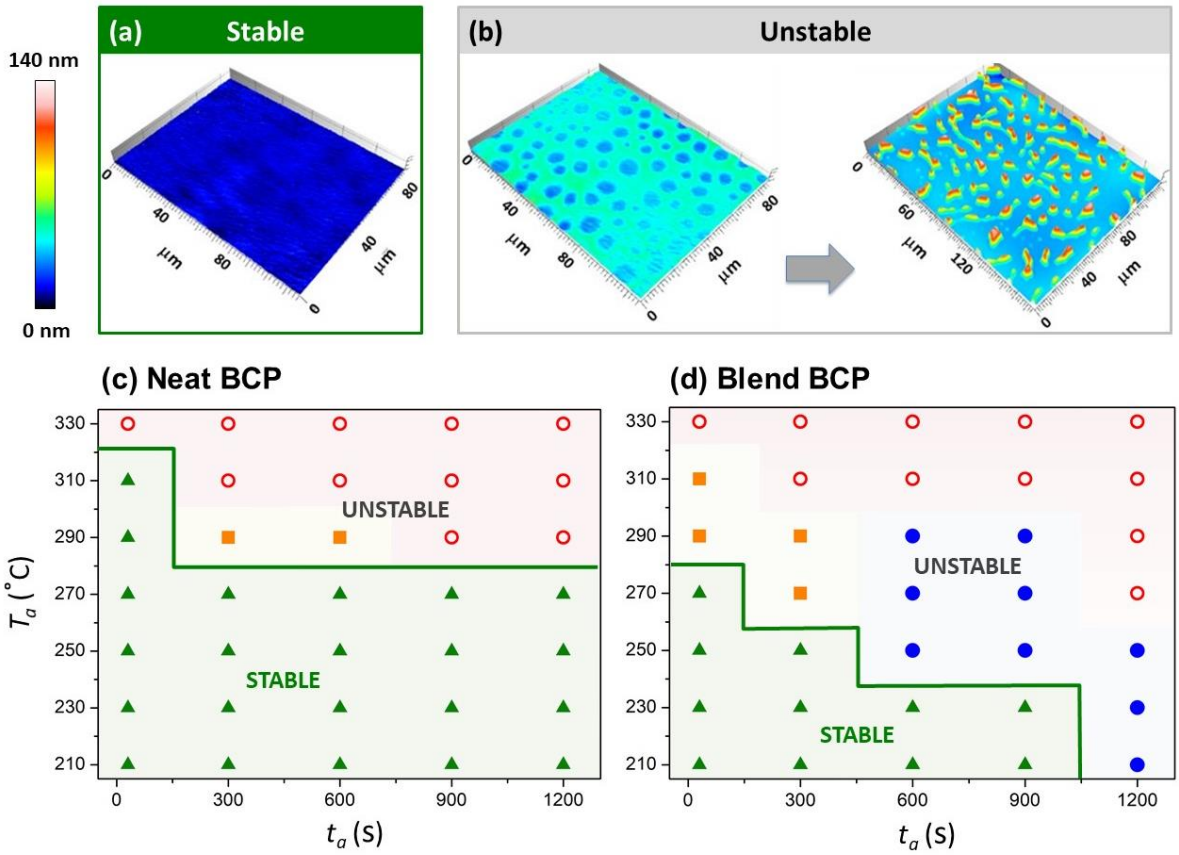

Figure 1. Optical profilometry height maps describing the topography of the samples with stable (a) and unstable (b) conditions, respectively. Morphological and thermal stability diagram corresponding to the neat (c) and blend (d) BCP thin films as a function of the annealing temperature (T_a) and time (t_a): stable films (green triangles), early formation of topographic inhomogeneities (yellow squares), dewetting of the film with self-assembled lamellar nanostructures (blue full circles), dewetting of the film and disappearance of lamellar nanostructures (red empty circles).

To preliminary check whether the thermal stability of the samples impairs the morphological stability of the films, a thermogravimetric analysis coupled with gas chromatography-mass spectrometer (TGA-GC-MS) was carried out on neat BCP and blend BCP films.[23] Such analysis allows detecting the onset of thermal degradation by monitoring the temperature evolution of styrene (S, mass peaks at m/z= 104) and methyl methacrylate (MMA, mass peaks at m/z= 100). Figure 2 reports the TGA-GC-MS chromatograms

at a heating rate of 20 °C/min under nitrogen atmosphere. The sampling of the evolved gas from the TGA occurs every 30 s and, in this way, the gas evolution profiles have a resolution of 10 °C.

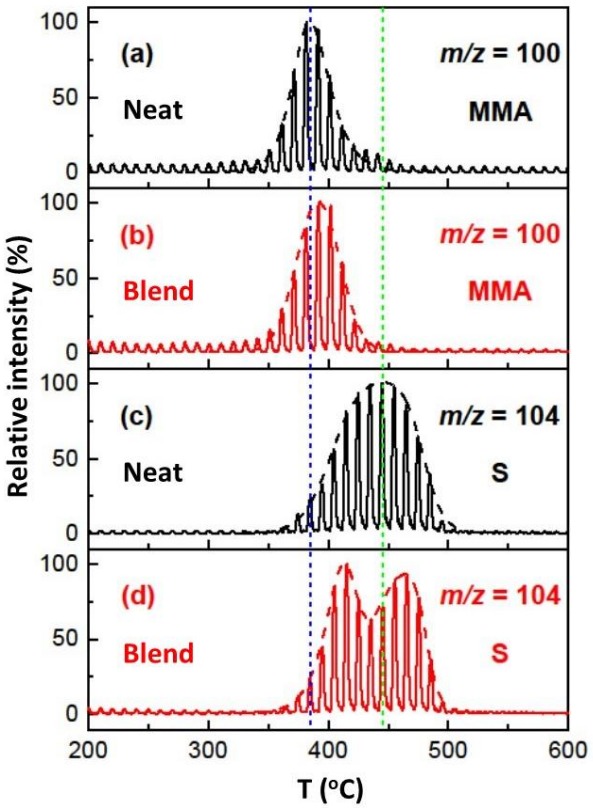

Figure 2. TGA-GC-MS chromatograms for neat BCP and blend BCP with reference to the mass peaks at m/z 100 and m/z 104 corresponding to methyl methacrylate (MMA) (a and b) and styrene (S) (c and d)) respectively. The vertical dashed lines representing the maximum loss temperature of methyl methacrylate (blue line) and styrene (green line) are included to guide the eyes.

The evolution of methacrylate in the neat BCP (Figure 2a) is quite similar to the one of the blend system, with the onset of degradation at about 330 °C with a maximum at 380 °C (blue dashed line in Figure 2). The release of styrene in neat BCP (Figure 2c) occurs with a maximum centered at 450°C with the loss profile spreading over a temperature range of approximately 150 °C. In contrast, two main loss peaks are observed for blend BCP (Figure 2d) due to the different thermal stability of the PS homopolymer and the corresponding block in the BCP.

The above data are in agreement with literature[31] where the thermal degradation of PS-b-PMMA as well as PS and PMMA is described to occur, in the same conditions adopted here, by an unzipping depolymerization mechanism. Since the thermal degradation of the neat BCP[32] and blend BCP occurs at temperatures definitely higher than those selected for the present investigation, we conclude that the various morphologies are unaffected by the thermal stability of the materials.

Stable condition- Long-range ordering

To outline the effect of blending BCP with homopolymers on the long-range ordering of the lamellar structures, the correlation length (ξ) was extracted from SEM micrographs of both neat BCP and blend BCP once subjected to various thermal treatments in the stable condition (green zone of Figures 1c and 1d). Figures 3a and 3b report the ξ values for neat BCP (ξ_{neat}) and blend BCP (ξ_{blend}) at different temperatures as a function of time. At t_a = 30 s, ξ_{neat} values comprised between 70 and 100 nm are obtained, depending on the annealing temperature. By increasing annealing time, a slight increase in ξ_{neat} is observed, reaching the maximum value of $\xi_{neat} \approx$ 130 nm corresponding to t_a = 900 s and T_a = 270 °C.

Growth exponents (τ) ranging from τ = 0.02 (for T_a = 210 °C) to τ = 0.06 (at T_a = 270 °C) are observed, indicating a slow coarsening kinetics. This smooth increase in ξ_{neat} with increasing time and temperature agrees with the behavior of several neat lamellar BCPs, thermally treated in RTP[28-33-34] or furnace[35-36] where growth exponents lower than 0.1 are observed for annealing times longer than 100 s and annealing temperatures below 270 °C.

The ξ_{blend} evolution is completely different from ξ_{neat}. At T_a of 230 and 250 °C (red circles and green triangles in Figure 3b respectively), even after short annealing times, ξ_{blend} of approximately 200 nm are observed (see also Figures 3c and 3d). Furthermore, a noticeable increase in ξ_{blend} occurs, reaching the maximum value of ξ_{blend} = 1120 nm for samples treated at T_a = 230 °C for t_a = 600 s (Figures 3e and S3). This correlation length value results one order of magnitude higher than the maximum value obtained with neat BCP. However, a consistent reduction in the temperature range of the stable region is observed

thus in turn reducing the processing window for the blend BCP system. In addition, even at the relatively low temperature of 230°C, a consistent decrease of ξ_{blend} occurs for long annealing time accompanied by the appearance of dark areas localized in correspondence of the defects in the lamellar pattern (red circles in Figure 3f). A similar behaviour was previously observed[37] and tentatively explained by the occurrence of a local order-disorder transition due to a change in the mass distribution of the homopolymers within the lamellar domains.

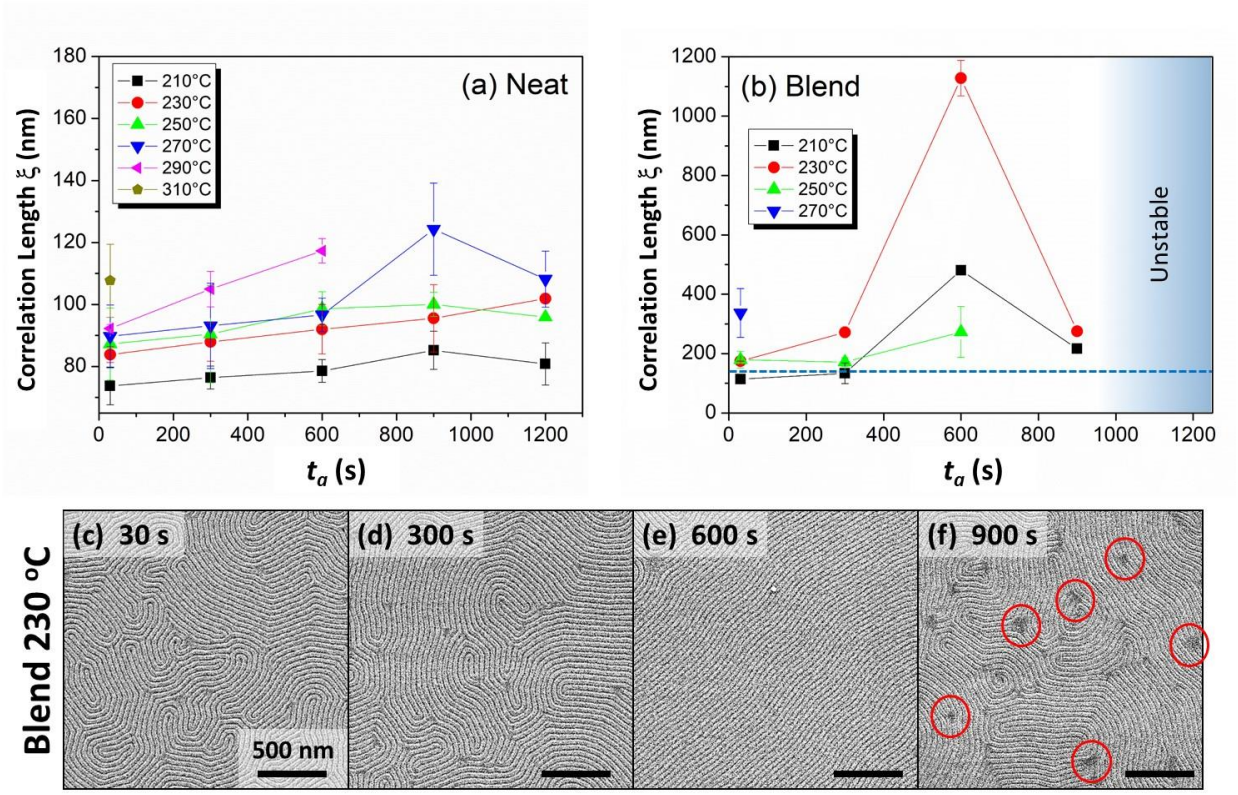

Figure 3. Correlation length as a function of annealing time (t_a) at different annealing temperatures for (a) neat BCP and (b) blend BCP sets. The blue dashed line in (b) represents the maximum value of ξ_{neat}. SEM images of blend BCP at 230°C annealed for different time periods are reported in (c)-(f).

The propensity of long range ordering of blend BCP and neat BCP was tested by performing the self-assembly process inside graphoepitaxy defined linear trenches, with variable width (W) between 0.9 μm and 5 μm, prepared by laser writer lithography (Figure 4). In neat BCP, the maximum correlation length

within graphoepitaxy defined trenches is equal to the one observed on the flat substrate (Figures 4a and 4c) in agreement to the general finding[38] that the maximum W useful to direct the self-assembly ordering of neat BCP is approximately equal to the correlation length measured on the flat surface ($W \approx \xi$). In contrast, the correlation length of blend BCP within the patterned structure is much higher than the one on the flat substrate leading to a monodomain extending above 3500 nm (Figures 4b and 4d). In the latter case the lamellae are aligned perpendicular to the trenches due to the presence of RCP on the side walls of the trenches.[39-40] However, it should be observed that several defects are present.

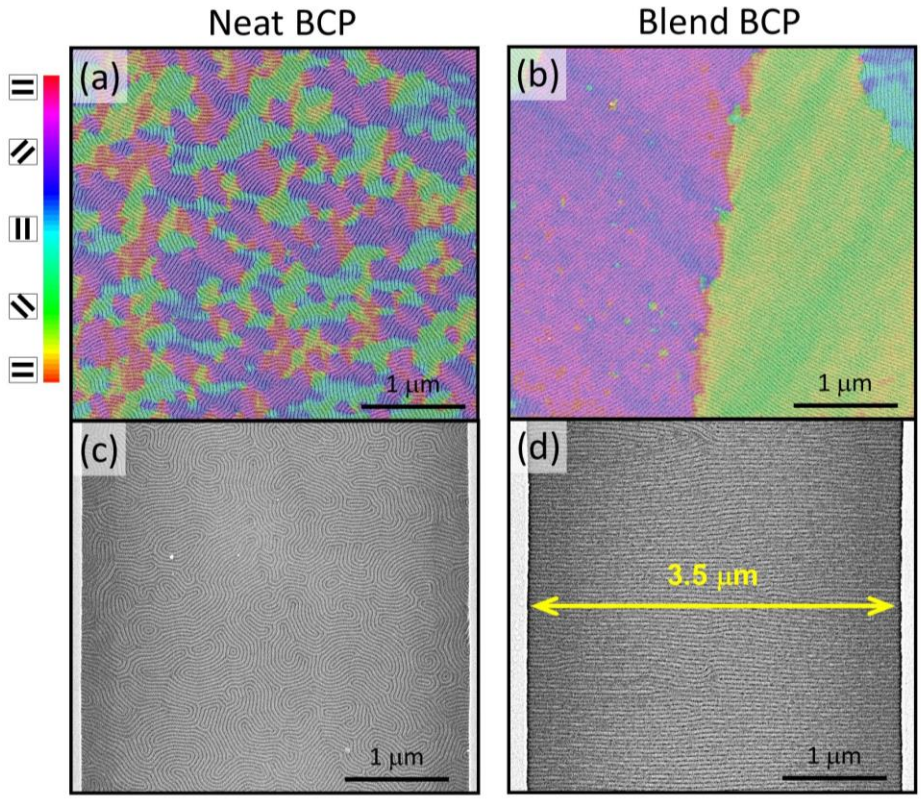

Figure 4. Neat BCP and blend BCP on the flat substrate (a and b) and inside the patterned structure (c and d). The samples were thermally treated at the annealing conditions that maximize the correlation length on the flat substrate (*i.e.* T_a = 270 °C and t_a = 900 s for the neat BCP and T_a = 230 °C and t_a = 600 s blend BCP). In Figures (a) and (b) the false colour map describing the orientation of lamellar structures are overlapped to the corresponding SEM micrographs.

Unstable condition - Nanoscale ordering

The characterization of films in the unstable region described in Figure 1 was performed by SEM and AFM at different magnifications (Figure 5). In samples treated for $t_a \leq 300$ s, the formation of areas of uneven thickness are observed (Figure 5a). The lower thickness areas are due to film breaking that leads to holes over the RCP grafted layer on the SiO_2 substrate. Starting from the edge of these holes, and proceeding for several micrometers, a continuous increase in the film thickness is generated. Finally, a thickness plateau region is reached, corresponding to the value of h = 70 nm (Figure 5b).

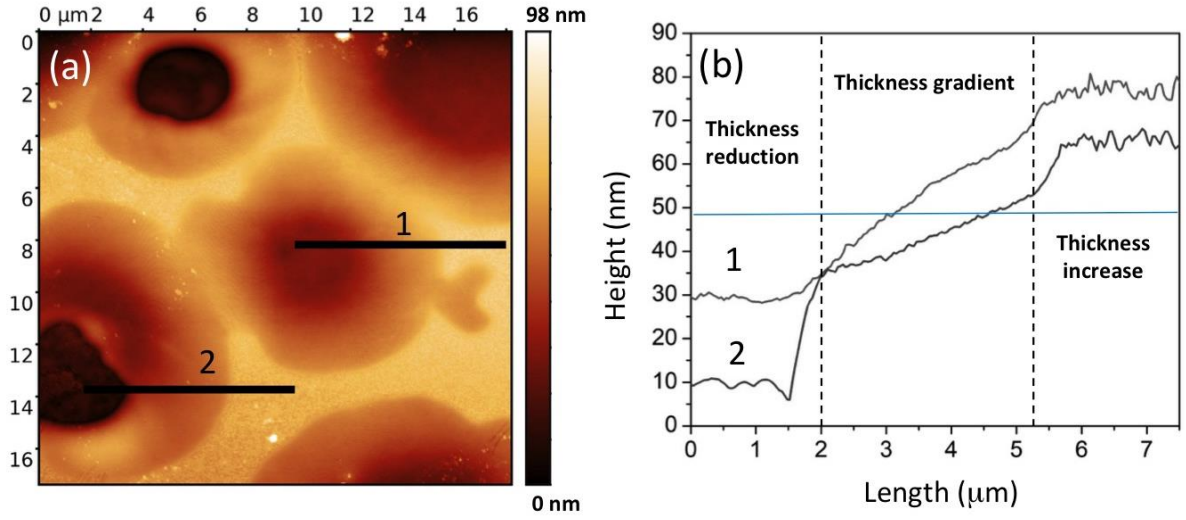

Figure 5: (a) AFM micrograph representing the surface topography in uneven blend BCP sample treated at T_a = 290 °C and t_a = 30 s. (b) Height profiles extracted in correspondence of the black lines 1 and 2 in (a).

In more detail, Figure 6a shows the AFM magnification of the zone straddling the thickens gradient and the thickness increase area, whereas Figure 6b reports the SEM image of the same zone in which the lines green and red define the parallel and perpendicular directions with respect to the lamellae. Starting from the middle of the hole, the film is almost flat (Figure 6c) in the perpendicular direction whereas a continuous increase in the film thickness is observed along the parallel direction (Figure 6d). In addition, on going from the edge of the hole to the plateau region, a peculiar morphological change occurs, as reported in the top right corner of Figure 6b. In the film region in which the thickness increases, a

lamellar morphology is observed, characterized by a very large correlation length due to the so-called "*geometrical anchoring*" phenomenon.[13-14] However, once the thickness plateau region is reached, the lamellar morphology disappears and circular features are seen with approximately 28 nm diameter as measured by the corresponding AFM height map reported in Figure S4.

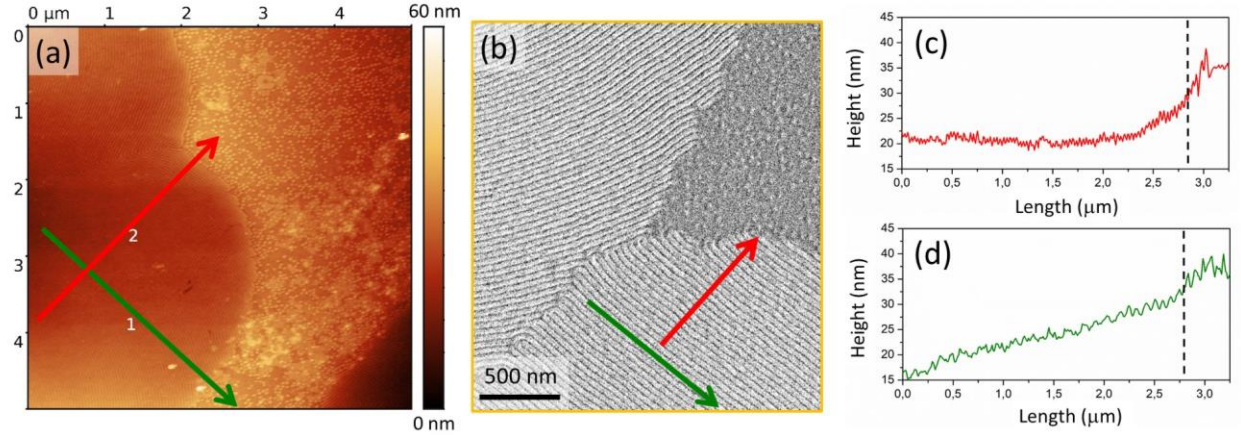

Figure 6: Geometric anchoring effect in of the SA lamellae in blend BCP described by (a) AFM and (b) SEM. The arrows in figure (a) and lines in figure (b) represent respectively the direction along (green) and across (red) the in-plane orientation of the lamellae. The height profiles extracted in correspondence of the red and green lines of the AFM micrograph (b) are reported in graphics (c) and (d).

A further increase in T_a or t_a induces a dewetting in both neat BCP and blend BCP samples and the morphology follows the typical phase sequence observed in the dewetting of thin polymer films, consisting in the formation of holes, bicontinuous patterns and droplets.[41] Two types of dewetted morphologies are seen, as illustrated in Figure 7. The first type of dewetted morphology, seen in both neat and blend systems, is characterized by the absence of SA lamellae patterns (see Figure 7a) due to the occurrence of the order-disorder transition. This morphology is marked in Figures 1c and 1d by red circles and occurs in correspondence to high temperatures and long annealing times.

The second type of dewetted morphology, observed in the region marked by the blue circles in Figures 1c and 1d corresponding to relatively lower temperatures and times, consists of droplets in which the lamellar structure is preserved (Figure 7b). The lamellae propagate across the whole thickness of the

dewetted features as demonstrated by the perfect replication of the lamellar structure after sequential infiltration synthesis (SIS) of TiO_2. These low temperature dewetted features are observed only in blend BCP, starting from films of 40 nm thickness, whereas for neat BCP the occurrence of low temperature dewetting process was observed only in films with h < 10 nm.[42,43,44]. As thermally activated dewetting typically occurs in the regime of confined thin films[45] (*i.e.* h lower than two times the radius of gyration R_g of the unperturbed molecules), this experimental finding indicates that the presence of low molar mass homopolymers substantially reduces the stability of the films.

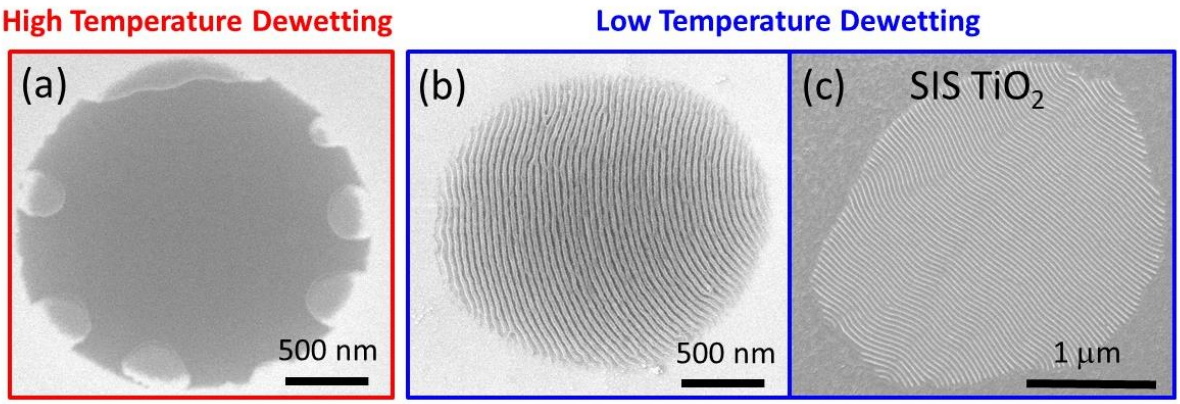

Figure 7. (a) SEM micrograph showing the morphology of a droplet dewetted in blend BCP at high temperature (T_a = 310 °C and t_a = 1200 s). (b) Nanoscale morphology of BCP films dewetted at low temperature (T_a = 250 °C and t_a = 1200 s). (c) SEM micrograph showing the lamellar features after sequential infiltration synthesis of TiO_2 inside a droplet dewetted at low temperature.

Similar to what observed in inhomogenous samples, the remarkable ordering of the nanometric lamellae inside the dewetted droplets (Figures 7b and 7c) are ascribed to the *geometric anchoring* effect induced by the presence of a gradient thickness. Kim and co-workers observed that the spontaneous alignment along the gradient direction becomes efficient when the dewetted features reach a critical angle θ > 3-5° and thickness h > 500 nm.[14] Within these geometric conditions, annihilation of linear defects, dislocations and disclinations, is favoured and reorientation of the lamellae along the thickness gradient occurs. On the

contrary, for h < 500 nm the *geometric anchoring* effect becomes inefficient and the lamellae are randomly oriented on the substrate.

In the present case, AFM analysis (Figures 8a and S5) performed on blend BCP dewetted at low temperature (T_a = 250 °C and t_a = 1200 s) reveals the formation of droplets with contact angle θ_{blend} = 6.5° and h < 100 nm (Figure 8b).

To establish whether the high ordering observed in blend BCP droplets is induced by the geometric anchoring or by the presence of low molar mass homopolymers, it would be necessary to compare the lamellar structure inside droplets with the same geometrical characteristics obtained with the neat BCP and with the blend BCP. However, the low temperature dewetting was never observed in neat BCP films. Consequently, a dewetted structure for the neat BCP was artificially obtained by inducing the self-assembly process over linear trenches. Figures 8c and 8d show the formation of a dewetted structure confined between tranches for the neat BCP featuring a contact angle (θ_{neat} = 6.0°) similar to that of blend BCP (θ_{blend} = 6.5°). As a multidomain structure is observed for neat BCP dewetted within the tranches, the ordering degree results definitely lower than that observed for the blend in the droplets. The described experiment clearly indicates that the high lamellar ordering for blend BCP is due to the presence of the low molar mass homopolymers, that extends the efficiency of the *geometric anchoring* towards much smaller thicknesses than those reported in literature.

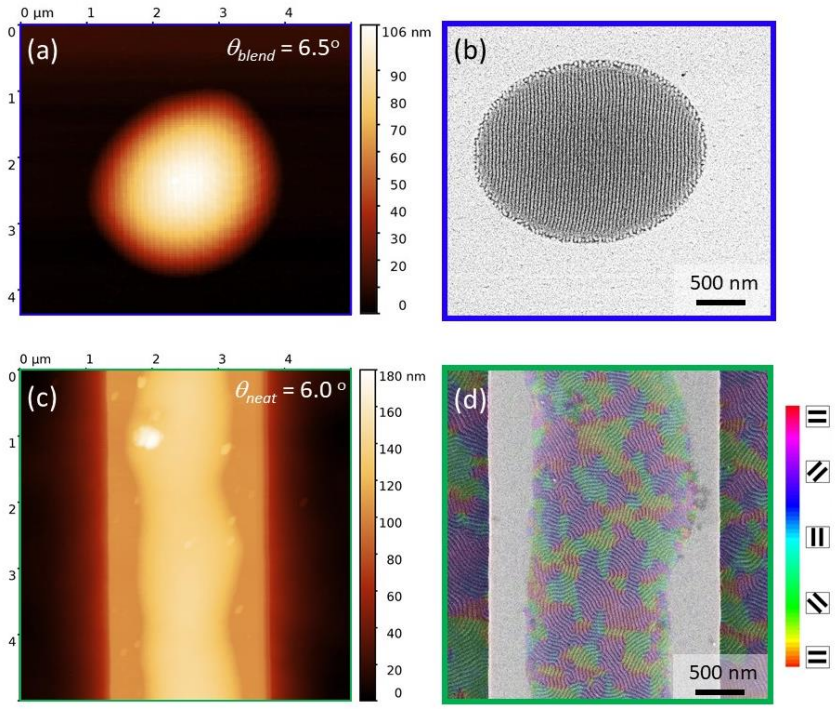

Figure 8. SEM micrographs and AFM height maps describing the *geometric anchoring* effect in neat (a and b) and blend (c and d) BCP films, thermally treated at T_a = 250 °C and t_a = 900 s. The dewetting of neat BCP (c)-(d) was induced by the presence of linear trenches. The false colour map representing the orientation of the lamellae are overlapped to the SEM micrograph (b).

Mechanism of low and high temperature dewetting

According to literature,[45] the three main dewetting mechanisms, namely heterogeneous nucleation, homogeneous nucleation or spinodal dewetting, can be distinguished by applying a two-dimensional Fourier transform (2D-FFT) to the SEM or optical profilometer micrographs representing the topography of the samples, and evaluating the appearance of intensity rings, associated to the presence of in-plane prominent lengths λ (See figure S6).

The heterogeneous nucleation mechanism occurs when impurities, such as dust or small particles, produce local changes in the film thickness, thus leading to the formation of randomly distributed patterns with similar lateral dimension (*e.g.* formation of holes with same diameter around the dust particles). The

random nature of the pattern distribution suppresses the formation of intensity rings in the 2D-FFT and, accordingly, no prominent λ is detectable. The other two mechanisms can be differentiated following the evolution of λ as a function of time and film thickness h.

In the present system, film initially in the stability region presents a flat surface. Dewetted areas only appear in correspondence of dust particles, as shown in the case of a blend BCP film treated at T_a = 250 °C and t_a = 300 s (Figure 9a). No prominent λ is detected thus indicating the occurrence of dewetting *via* the heterogeneous nucleation mechanism.

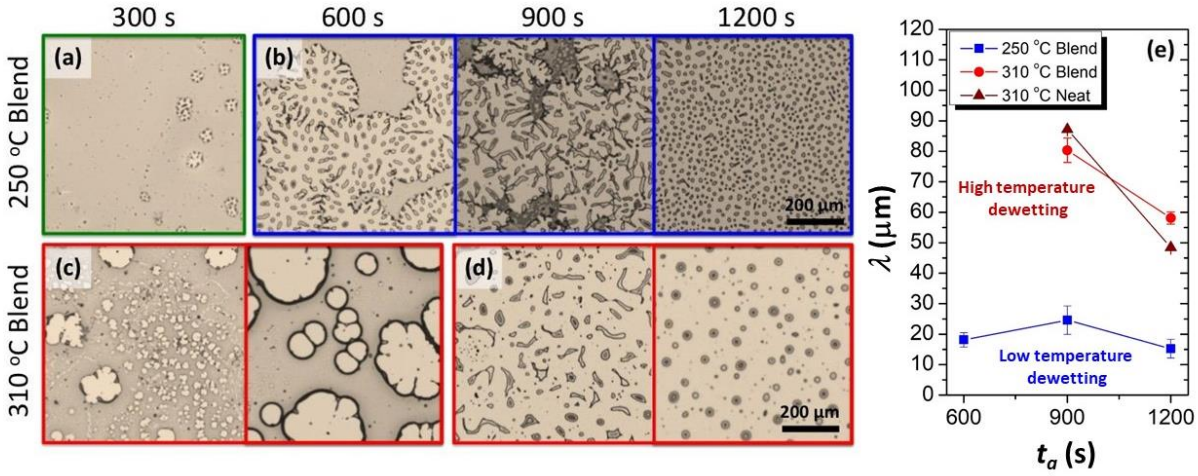

Figure 9. Optical microscopy images for blend BCP films treated at T_a = 250 °C (a and b) and T_a = 310 °C (c and d) for different t_a between 300 and 1200 s. Trend of in-plane λ as a function of time at different temperatures for neat BCP and blend BCP (e).

When dewetting occurs at the low temperature dewetting conditions, as is the case of blend BCP at 250°C (Figure 9b), the 2D-FFT presents well-detectable λ values comprised between 10 and 20 µm (blue squares in Figure 9e). In contrast, at the high temperature dewetting condition ($T_a \geq$ 310 °C and $t_a \leq$ 600), holes with different size appear for both neat BCP (Figure S8) and blend BCP (Figure 9c), indicating a

homogeneous nucleation mechanism. Moreover, at $t_a \geq 900$ s (Figure 9d) λ values three times higher than those for low temperature conditions are observed (red circles and triangles in Figure 9e).

As the occurrence of prominent lengths λ suggests a spinodal dewetting mechanism, blend BCP samples with thickness h comprised between 10 and 43 nm were prepared and annealed at T_a = 250 or 310 °C for 900 s. Figure 10 reports λ as a function of h for both temperatures whereas the corresponding intensity profiles obtained after radial averaging of the 2D-FFT are reported in Figures S7a and S7b. A significant increase in λ is observed as the annealing temperature increases with growth exponent ε of 1.26 at 250 °C and 1.24 at 310 °C. The nearly identical ε values suggest that the dewetting mechanism is the same at both temperatures irrespective from the presence (at 250°C) and absence (at 310°C) of the nanometric lamellar structure.

Previous literature reports growth exponents $\varepsilon \sim 1$ for films of blends consisting of deuterated PS and polyparamethylstyrene, with thickness exceeding $h > 2 \cdot R_g$, while in the confined regime $h < 2 \cdot R_g$ the instability was described as governed by spinodal dewetting with $\varepsilon \sim 2$.[46] In case of block copolymers treated at T_a below the ODT, stable films not subjected to rupture process are observed when $h > 2 \cdot R_g$. In contrast, when $h < 2 \cdot R_g$ dewetting processes occurs with $\varepsilon \sim 1$.[47,48] This behaviour suggested the occurrence of an additional stabilizing effect of the BCP nanometric morphology for $h > 2 \cdot R_g$.

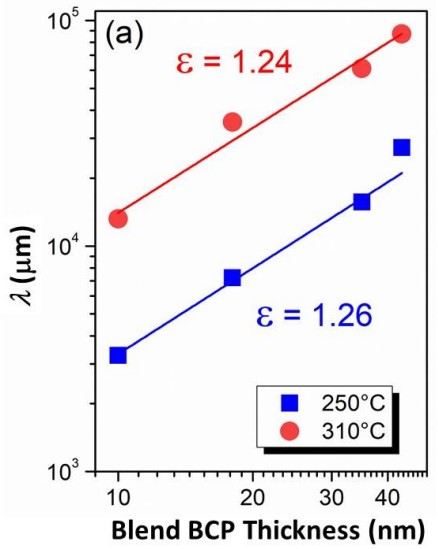

Figure 10: Characteristic λ as a function of the blend BCP thickness treated at 250 °C (blue squares) and 310 °C (red dots).

In the present blend BCP system, the presence of low M_n homopolymers reduces the stabilizing effect of the SA lamellae leading to instability for $h > 2 \cdot R_g$ with a growth exponent not depending on h and at the same time inhibits the spinodal behavior in the confined regime $h < 2 \cdot R_g$. The observation that the same dewetting mechanism is operating in presence (250 °C) and absence (310 °C) of the BCP lamellar structure further confirms the reduced stabilization brought about by the BCP supramolecular structure when low molar mass homopolymers are present.

Low temperature dewetting of unstable blend BCPs represents an intriguing solution to generate plasmonics and photonics structures. A fundamental requirement is the control over the position and size of the dewetted features. However, when low temperature dewetting is induced over a flat unpatterned surface, the obtained features randomly arrange on the substrate (left zone in Figure 11a). To overcome such limitation, the dewetting process can be replicated over periodic chemical or topographic patterns.[11,47,42] Accordingly, BCP/homopolymer ternary blend solutions were spin coated over periodic patterns consisting in an array of micrometric squares (Figure 11b), previously neutralized with a RCP layer. The samples were then thermally treated at T_a = 270 °C and t_a = 600 s to induce low temperature dewetting. After the thermal treatment, the formation of droplets periodically distributed within the pre-patterned structures is observed (Figures 11b and 11c). As previously reported, the height of the droplets linearly scales with their diameter,[47] thus the maximum height reached by the droplet shown in Figure 11c is ~ 95 nm.

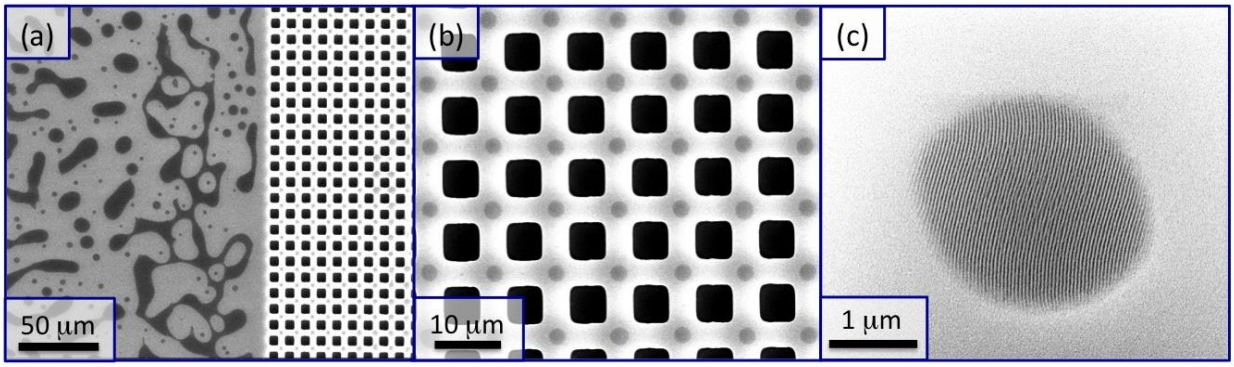

Figure 11: SEM micrographs at different magnifications describing the hierarchical assembly of lamellar structure obtained over squared graphoepitaxy patterns of 5 µm side. The micrograph (a) represents a zone across the border between the flat part of the sample (left zone) and the periodic pattern (right zone).

CONCLUSIONS

The morphological stability and ordering characteristics of a lamellae forming poly(styrene-block-methyl methacrylate) (PS-b-PMMA) block copolymer (BCP), either alone or blended with low molar mass polystyrene (PS) and polymethylmethacrylate (PMMA) homopolymers, were investigated. An increase of one order of magnitude occurs in the correlation length of the lamellar nano-domains of blend BCP with respect to neat BCP. Moreover, a morphological instability of blend BCP is observed and results in dewetting of relatively thick films with the formation of micrometric size areas. Consequently, the dewetting of blend BCP within a periodic pattern leads to highly ordered hierarchical structures featuring substantial thickness-modulation. These may find applications in fields requiring a discrete number of highly ordered nanowires periodically arranged in a thickness-modulated nanometric pattern for the realization of plasmonic surfaces[50-51-52] or photonic structures.[53-54-55]

ASSOCIATED CONTENT

Supporting Information

The Supporting Information is available free of charge at http://pubs.acs.org.

Additional SEM micrographs representing the surface morphology of neat and blend BCP treated in RTP with annealing time and temperatures ranging from 30 to 900 s and from 210 to 330 C°, the grain size and the long-range ordering of the blend BCP treated at T_a = 230 °C for t_a = 600 s, AFM height map of the dewetted droplets, description of the procedure used for the calculation of the PSD functions.

ACKNOWLEDGEMENTS

The project 16ENV07 Aeromet has received funding from the EMPIR programme co-financed by the Participating States and from the European Union's Horizon 2020 research and innovation programme.

SEM characterisation has been performed at NanofacilityPiemonte in INRiM, a laboratory supported by Compagnia di San Paolo Foundation.

REFERENCES

(1) Zhang, X.; Sushkov, A. B.; Metting, C. J.; Fackler, S.; Drew, H. D.; Briber, R. M. Silicon Patterning Using Self-Assembled PS-b-PAA Diblock Copolymer Masks for Black Silicon Fabrication via Plasma Etching. *Plasma Process. Polym.* **2012**, *9* (10), 968–974.

(2) Dolan, J. A.; Wilts, B. D.; Vignolini, S.; Baumberg, J. J.; Steiner, U.; Wilkinson, T. D. Optical Properties of Gyroid Structured Materials: From Photonic Crystals to Metamaterials. *Adv. Opt. Mater.* **2015**, *3* (1), 12–32.

(3) Vukovic, I.; Brinke, G. Ten; Loos, K. Block Copolymer Template-Directed Synthesis of Well-Ordered Metallic Nanostructures. *Polymer* **2013**, *54* (11), 2591–2605.

(4) Stefi, M.; Guldin, S. Block Copolymer Self-Assembly for Nanophotonics. *Chem. Soc. Rev.* **2015**, *44* (15), 5076--5091.

(5) Choi, S. Y.; Lee, C.; Lee, J. W.; Park, C.; Kim, S. H. Dewetting-Induced Hierarchical Patterns in

Block Copolymer Films. *Macromolecules* **2012**, *45* (3), 1492–1498.

(6) Kim, T. H.; Hwang, J.; Hwang, W. S.; Huh, J.; Kim, H. C.; Kim, S. H.; Hong, J. M.; Thomas, E. L.; Park, C. Hierarchical Ordering of Block Copolymer Nanostructures by Solvent Annealing Combined with Controlled Dewetting. *Adv. Mater.* **2008**, *20* (3), 522–527.

(7) Brassat, K.; Kool, D.; Bürger, J.; Lindner, J. K. N. Hierarchical Nanopores Formed by Block Copolymer Lithography on the Surfaces of Different Materials Pre-Patterned by Nanosphere Lithography. *Nanoscale* **2018**, *10* (21), 10005–10017.

(8) Zaluzec, N. J.; Kim, D. H.; Ocola, L. E.; Nealey, P. F.; Suh, H. S.; Gleason, K. K.; Xiong, S.; Moni, P. Sub-10-Nm Patterning via Directed Self-Assembly of Block Copolymer Films with a Vapour-Phase Deposited Topcoat. *Nat. Nanotechnol.* **2017**, *12* (6), 575–581.

(9) Park, S.; Lee, D. H.; Xu, J.; Kim, B.; Hong, S. W.; Jeong, U.; Xu, T.; Russell, T. P. Macroscopic 10-Terabit-per-Square-Inch Arrays from Block Copolymers with Lateral Order. *Science* **2009**, *323* (February), 1030–1033.

(10) Onses, M. S.; Song, C.; Williamson, L.; Sutanto, E.; Ferreira, P. M.; Alleyne, A. G.; Nealey, P. F.; Ahn, H.; Rogers, J. A. Hierarchical Patterns of Three-Dimensional Block-Copolymer Films Formed by Electrohydrodynamic Jet Printing and Self-Assembly. *Nat. Nanotechnol.* **2013**, *8* (9), 667–675.

(11) Farrell, R. A.; Kehagias, N.; Shaw, M. T.; Reboud, V.; Zelsmann, M.; Holmes, J. D.; Sotomayor Torres, C. M.; Morris, M. A. Surface-Directed Dewetting of a Block Copolymer for Fabricating Highly Uniform Nanostructured Microdroplets and Concentric Nanorings. *ACS Nano* **2011**, *5* (2), 1073–1085.

(12) Basutkar, M. N.; Majewski, P. W.; Doerk, G. S.; Toth, K.; Osuji, C. O.; Karim, A.; Yager, K. G. Aligned Morphologies in Near-Edge Regions of Block Copolymer Thin Films. *Macromolecules* **2019**, *52*, 7224–7233.

(13) Bong, B.; Kim, H.; Shin, D. O.; Jeong, S.; Koo, C. M.; Jeon, S. C.; Hwang, W. J.; Lee, S.; Lee, M. G.; Kim, S. O. Hierarchical Self-Assembly of Block Copolymers for Lithography-Free

Nanopatterning. *Adv. Mater.* **2008**, *20*, 2303–2307.

(14) Kim, B. H.; Lee, H. M.; Lee, J. H.; Son, S. W.; Jeong, S. J.; Lee, S.; Lee, D. I.; Kwak, S. U.; Jeong, H.; Shin, H.; Yoon, J. B.; Lavrentovich, O. D.; Kim, S. O. Spontaneous Lamellar Alignment in Thickness-Modulated Block Copolymer Films. *Adv. Funct. Mater.* **2009**, *19* (16), 2584–2591.

(15) Doerk, G. S.; Li, R.; Fukuto, M.; Rodriguez, A.; Yager, K. G. Thickness-Dependent Ordering Kinetics in Cylindrical Block Copolymer/Homopolymer Ternary Blends. *Macromolecules* **2018**, *51* (24), 10259–10270.

(16) Stuen, K. O.; Thomas, C. S.; Liu, G.; Ferrier, N.; Nealey, P. F. Dimensional Scaling of Cylinders in Thin Films of Block Copolymer-Homopolymer Ternary Blends. *Macromolecules* **2009**, *42* (14), 5139–5145.

(17) Stoykovich, M. P. Directed Assembly of Block Copolymer Blends into Nonregular Device-Oriented Structures. *Science* **2005**, *308* (5727), 1442–1446.

(18) Torikai, N.; Takabayashi, N.; Noda, I.; Koizumi, S.; Morii, Y.; Matsushita, Y. Lamellar Domain Spacings of Diblock Copolymer/Homopolymer Blends and Conformations of Block Chains in Their Microdomains. *Macrolecules* **1997**, *30* (96), 5698–5703.

(19) Kim, J. Y.; Jin, H. M.; Jeong, S.; Chang, T.; Kim, B. H.; Cha, S. K.; Kim, J. S.; Shin, D. O.; Choi, J. Y.; Kim, J. H.; et al. Bimodal Phase Separated Block Copolymer/Homopolymer Blends Self-Assembly for Hierarchical Porous Metal Nanomesh Electrodes. *Nanoscale* **2018**, *10*, 100–108.

(20) Son, S.-W.; Shin, J.; Kim, J. Y.; Jin, H. M.; Park, S. J.; Kim, S. O.; Kim, J. U.; Kim, B. H.; Kim, M.-H.; Koo, C. M. Anomalous Rapid Defect Annihilation in Self-Assembled Nanopatterns by Defect Melting. *Nano Lett.* **2015**, *15* (2), 1190–1196.

(21) Cho, A.; La, Y.; Jeoung, S.; Moon, H. R.; Ryu, J. H.; Shin, T. J.; Kim, K. T. Mix-and-Match Assembly of Block Copolymer Blends in Solution. *Macromolecules* **2017**, *50* (8), 3234–3243.

(22) Hur, S. M.; Thapar, V.; Ramírez-Hernández, A.; Nealey, P. F.; De Pablo, J. J. Defect Annihilation Pathways in Directed Assembly of Lamellar Block Copolymer Thin Films. *ACS Nano* **2018**, 12, 10, 9974–9981.

(23) Gianotti, V.; Antonioli, D.; Sparnacci, K.; Laus, M.; Giammaria, T. J.; Ceresoli, M.; Ferrarese Lupi, F.; Seguini, G.; Perego, M. Characterization of Ultra-Thin Polymeric Films by Gas Chromatography-Mass Spectrometry Hyphenated to Thermogravimetry. *J. Chromatogr. A* **2014**, *1368*, 204–210.

(24) Sparnacci, K.; Antonioli, D.; Gianotti, V.; Laus, M.; Ferrarese Lupi, F.; Giammaria, T. J.; Seguini, G.; Perego, M. Ultrathin Random Copolymer-Grafted Layers for Block Copolymer Self-Assembly. *ACS Appl. Mater. Interfaces* **2015**, *7* (20), 10944–10951.

(25) Peng, Q.; Tseng, Y.; Darling, S. B.; Elam, J. W. A Route to Nanoscopic Materials via Sequential Infiltration Synthesis on Block Copolymer Templates. *ACS Nano* **2011**, *5* (6), 4600–4606.

(26) Tseng, Y. C.; Peng, Q.; Ocola, L. E.; Elam, J. W.; Darling, S. B. Enhanced Block Copolymer Lithography Using Sequential Infiltration Synthesis. *J. Phys. Chem. C* **2011**, *115* (36), 17725–17729.

(27) Harrison, C.; Adamson, D. H.; Cheng, Z.; Sebastian, J. M.; Sethuraman, S.; Huse, D. A.; Register, R. A. Mechanisms of Ordering in Striped Patterns. *Science* **2000**, *290*, 1558–1560.

(28) Ferrarese Lupi, F.; Giammaria, T. J.; Ceresoli, M.; Seguini, G.; Sparnacci, K.; Antonioli, D.; Gianotti, V.; Laus, M.; Perego, M. Rapid Thermal Processing of Self-Assembling Block Copolymer Thin Films. *Nanotechnology* **2013**, *24* (31).

(29) Ferrarese Lupi, F.; Giammaria, T. J.; Seguini, G.; Ceresoli, M.; Perego, M.; Antonioli, D.; Gianotti, V.; Sparnacci, K.; Laus, M. Flash Grafting of Functional Random Copolymers for Surface Neutralization. *J. Mater. Chem. C* **2014**, *2* (25), 4909–4917.

(30) Stoykovich, M. P.; Edwards, E. W.; Solak, H. H.; Nealey, P. F. Phase Behavior of Symmetric Ternary Block Copolymer-Homopolymer Blends in Thin Films and on Chemically Patterned Surfaces. *Phys. Rev. Lett.* **2006**, *97* (14), 4–7.

(31) Bate, D. M.; Lehrle, R. S. Thermal Degradation of Polymer Blends: Polystyrene/PMMA Blend Behaviour Related to the Copolymerization Φ-Factor for This System. *Polym. Degrad. Stab.* **1997**, *55* (3), 295–299.

(32) Gianotti, V.; Antonioli, D.; Sparnacci, K.; Laus, M.; Giammaria, T. J.; Ferrarese Lupi, F.; Seguini, G.; Perego, M. On the Thermal Stability of PS-b-PMMA Block and P(S-r-MMA) Random Copolymers for Nanopatterning Applications. *Macromolecules* **2013**, *46* (20), 8224–8234.

(33) Ceresoli, M.; Ferrarese Lupi, F.; Seguini, G.; Sparnacci, K.; Gianotti, V.; Antonioli, D.; Laus, M.; Boarino, L.; Perego, M. Evolution of Lateral Ordering in Symmetric Block Copolymer Thin Films upon Rapid Thermal Processing. *Nanotechnology* **2014**, *25* (27).

(34) Ceresoli, M.; Volpe, F. G.; Seguini, G.; Antonioli, D.; Gianotti, V.; Sparnacci, K.; Laus, M.; Perego, M. Scaling of Correlation Length in Lamellae Forming PS-b-PMMA Thin Films upon High Temperature Rapid Thermal Treatments. *J. Mater. Chem. C* **2015**, *3* (33), 8618–8624.

(35) Ruiz, R.; Sandstrom, R. L.; Black, C. T. Induced Orientational Order in Symmetric Diblock Copolymer Thin Films. *Adv. Mater.* **2007**, *19* (4), 587–591.

(36) Ruiz, R.; Bosworth, J. K.; Black, C. T. Effect of Structural Anisotropy on the Coarsening Kinetics of Diblock Copolymer Striped Patterns. *Phys. Rev. B - Condens. Matter Mater. Phys.* **2008**, *77* (5), 1–5.

(37) Doerk, G. S.; Yager, K. G. Rapid Ordering in "Wet Brush" Block Copolymer/Homopolymer Ternary Blends. *ACS Nano* **2017**, *11* (12), 12326–12336.

(38) Aprile, G.; Ferrarese Lupi, F.; Fretto, M.; Enrico, E.; De Leo, N.; Boarino, L.; Volpe, F. G.; Seguini, G.; Sparnacci, K.; Gianotti, V.; et al. Toward Lateral Length Standards at the Nanoscale Based on Diblock Copolymers. *ACS Appl. Mater. Interfaces* **2017**, *9* (18).

(39) Ferrarese Lupi, F.; Giammaria, T. J.; Seguini, G.; Laus, M.; Enrico, E.; De Leo, N.; Boarino, L.; Ober, C. K.; Perego, M. Thermally Induced Orientational Flipping of Cylindrical Phase Diblock Copolymers. *J. Mater. Chem. C* **2014**, *2* (12), 2175–2182.

(40) Kim, M.; Han, E.; Sweat, D. P.; Gopalan, P. Interplay of Surface Chemical Composition and Film

Thickness on Graphoepitaxial Assembly of Asymmetric Block Copolymers. *Soft Matter* **2013**, *9* (26), 6135.

(41) Becker, J.; Grün, G.; Seemann, R.; Mantz, H.; Jacobs, K.; Mecke, K. R.; Blossey, R.; Mathematik, A.; Bonn, U.; Bonn, D.-. Complex Dewetting Scenarios Captured by Thin-Film Models. *Nat. Mater.* **2003**, *2*, 59–63.

(42) Seemann, R.; Herminghaus, S.; Jacobs, K. Dewetting Patterns and Molecular Forces: A Reconciliation. *Phys. Rev. Lett.* **2001**, *86* (24), 5534–5537.

(43) Ferrarese Lupi, F.; Giammaria, T. J. J.; Volpe, F. G. G.; Lotto, F.; Seguini, G.; Pivac, B.; Laus, M.; Perego, M.; Lupi, F. F.; Giammaria, T. J. J.; et al. High Aspect Ratio PS-b-PMMA Block Copolymer Masks for Lithographic Applications. *ACS Appl. Mater. Interfaces* **2014**, *6* (23), 21389–21396.

(44) Limary, R.; Green, P. F. Dewetting Instabilities in Thin Block Copolymer Films: Nucleation and Growth. *Langmuir* **1999**, *15* (17), 5617–5622.

(45) Muller-Buschbaum, P.; Bauer, E.; Wunnicke, O.; Stamm, M. The Control of Thin Film Morphology by the Interplay of Dewetting , Phase Separation and Microphase. *J. Phys. Condens. Matter* **2005**, *17*, S363–S386.

(46) Muller-Buschbaum, P.; Stamm, M. Film Thickness Dependence of the Domain Size in Weakly Incompatible Thin Polymer Blend Films. *Colloid Polym. Sci.* **2001**, *279*, 376–381.

(47) Ferrarese Lupi, F.; Giammaria, T. J.; Miti, A.; Zuccheri, G.; Carignano, S.; Sparnacci, K.; Seguini, G.; De Leo, N.; Boarino, L.; Perego, M.; et al. Hierarchical Order in Dewetted Block Copolymer Thin Films on Chemically Patterned Surfaces. *ACS Nano* **2018**, *12* (7), 7076–7085.

(48) Muller-Buschbaum, P.; Wolkenhauer, M.; Wunnicke, O.; Stamm, M.; Cubitt, R.; Petry, W. Structure Formation in Two-Dimensionally Confined Diblock Copolymer Films. *Langmuir* **2001**, *17*, 5567–5575.

(49) Brassat, K.; Lindner, J. K. N. Nanoscale Block Copolymer Self-Assembly and Microscale Polymer Film Dewetting : Progress in Understanding the Role of Interfacial Energies in the

Formation of Hierarchical Nanostructures. *Adv. Mater. Interfaces* **2020**, *7* (1901565).

(50) Koenderink, A. F. Plasmon Nanocavity Array Lasers: Cooperating over Losses and Competing for Gain. *ACS Nano* **2019**, *13* (7), 7377–7382.

(51) Dolan, J. A.; Dehmel, R.; Demetriadou, A.; Gu, Y.; Wiesner, U.; Wilkinson, T. D.; Gunkel, I.; Hess, O.; Baumberg, J. J.; Steiner, U.; et al. Metasurfaces Atop Metamaterials: Surface Morphology Induces Linear Dichroism in Gyroid Optical Metamaterials. *Adv. Mater.* **2019**, *31* (2).

(52) Baek, K. M.; Kim, J. M.; Jeong, J. W.; Lee, S. Y.; Jung, Y. S. Sequentially Self-Assembled Rings-in-Mesh Nanoplasmonic Arrays for Surface-Enhanced Raman Spectroscopy. *Chem. Mater.* **2015**, *27*, 5001–5013.

(53) Kim, J. Y.; Kim, H.; Kim, B. H.; Chang, T.; Lim, J.; Jin, H. M.; Mun, J. H.; Choi, Y. J.; Chung, K.; Shin, J.; et al. Highly Tunable Refractive Index Visible-Light Metasurface from Block Copolymer Self-Assembly. *Nat. Commun.* **2016**, *7*, 1–9.

(54) Brassat, K.; Assion, F.; Hilleringmann, U.; Lindner, J. K. N. Self-Organization of Nanospheres in Trenches on Silicon Surfaces. *Phys. Status Solidi Appl. Mater. Sci.* **2013**, *210* (8), 1485–1489.

(55) Wu, J.; Liow, C.; Tao, K.; Guo, Y.; Wang, X.; Miao, J. Large-Area Sub-Wavelength Optical Patterning via Long-Range Ordered Polymer Lens Array. *ACS Appl. Mater. Interfaces* **2016**, *8*, 16368–16378.